





Photodissociation Spectroscopy

How to cite:

International Edition: doi.org/10.1002/anie.201916493 German Editon: doi.org/10.1002/ange.201916493

Charge-Tagged DNA Radicals in the Gas Phase Characterized by UV/Vis Photodissociation Action Spectroscopy

Yue Liu, Andy Dang, Jan Urban, and František Tureček*

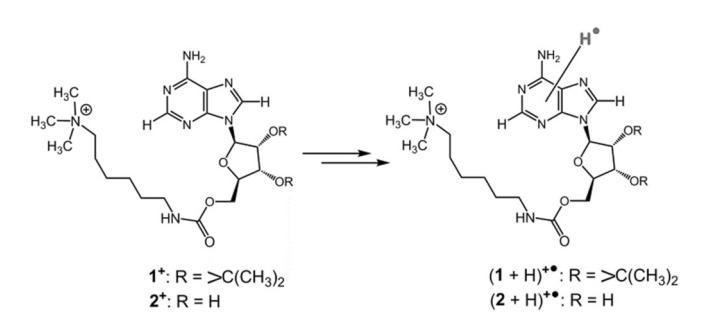
Abstract: Adenosine radicals tagged with a fixed-charge group were generated in the gas phase and structurally characterized by tandem mass spectrometry, deuterium labeling, and UV/Vis action spectroscopy. Experimental results in combination with Born–Oppenheimer molecular dynamics, ab initio, and excited-state calculations led to unambiguous assignment of adenosine radicals as N-7 hydrogen atom adducts. The charge-tagged radicals were found to be electronically equivalent to natural DNA nucleoside radicals.

Capture of secondary low-energy electrons by DNA is one of the major ionization processes leading to radical intermediates and triggering DNA damage. Previous studies using pulse radiolysis have revealed that electron adducts to nucleobases, nucleosides, and nucleotides underwent fast protonation by the solvent, forming neutral radicals as hydrogen atom adducts.^[1-5] The sites of hydrogen atom addition have been investigated by electron paramagnetic resonance spectroscopy, which revealed that the reaction products strongly depend on the environment conditions, such as pH and the concentration of metal ions. In particular, radical intermediates from pulse radiolysis of adenine, adenosine, and adenosine monophosphate have been studied by fast UV/Vis absorption spectroscopy and found to undergo consecutive reactions in solution and frozen glasses that complicated structure analysis.^[6–8]

An alternative approach to hydrogen atom adducts to nucleobases relies on a process that is a reversal of the radiolysis sequence in the condensed phase while largely avoiding consecutive and side reactions. Gas-phase or electrospray protonation of the nucleobase is first used to produce a cation in which the protonation site is determined by the topical gas-phase or solution basicity of the nucleobase, and can be controlled by the ionization conditions. In the next step, the cations are discharged by collisions with a gaseous electron donor, forming radicals that are analyzed by tandem mass spectrometry.^[9,10] While this approach worked well for nucleobases, the more complex oligonucleotide cation radicals formed by electron transfer underwent fast isomeriza-

tions by proton or hydrogen atom migrations between the nucleobases.^[11] To generate and characterize nucleoside radicals, which are the primary intermediates of relevance for the early stages of DNA damage, a different approach was needed.

We now report a new general approach to nucleoside radicals, as illustrated with adenosine, that circumvents the above-mentioned difficulties and allows spectroscopic investigations to be carried out. The nucleoside is furnished with a permanent-charge group forming a charged conjugate (Scheme 1). The conjugate is further charged by electrospray ionization, the doubly charged ion is selected by its m/z ratio and stored in a quadrupole ion trap. An ion-ion reaction with fluoranthene anion radical delivers the electron, reducing the dication into a cation radical which is again selected by its m/z and stored in the ion trap.



Scheme 1. Formation of adenosine radicals $(1 + H)^{+}$ and $(2 + H)^{+}$.

The cation radical is interrogated by UV/Vis photodissociation (UVPD) action spectroscopy, [12] which probes transitions in the valence-electron excitation region of 210–700 nm. By combining efficient ion preparation, selection, and manipulation in the ion trap with wavelength-resolved laser photodissociation, we achieve the first spectroscopic characterization of well-defined adenosine radicals. We also show that the charge-tagged radicals are electronically equivalent to natural DNA radicals, making this method suitable for generating and studying a variety of transient DNA intermediates.

Adenosine conjugates 1^+ and 2^+ were synthesized as shown in Scheme S1 (Supporting Information), and characterized by high-resolution and collision-induced dissociation tandem mass spectrometry, CID-MS², as described in the Suporting Information (Table S1, Figures S1 a,b and S2 a,b). We found that electron transfer to doubly charged $(2 + H)^{2+}$ (m/z 226.5) resulted in a near complete dissociation (Figure 1a) by loss of a H atom from the reduced adenine ring

Department of Chemistry, University of Washington

Seattle, WA 98195-1700 (USA)

E-mail: turecek@chem.washington.edu

Dr. J. Urban Metagenics, Inc.

Gig Harbor, WA 98332 (USA)

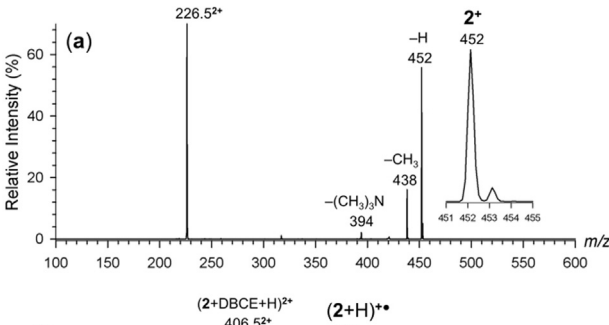
Supporting information and the ORCID identification number(s) for the author(s) of this article can be found under:

https://doi.org/10.1002/anie.201916493.

 $^{[^{\}star}]\,$ Y. Liu, Dr. A. Dang, Prof. Dr. F. Tureček







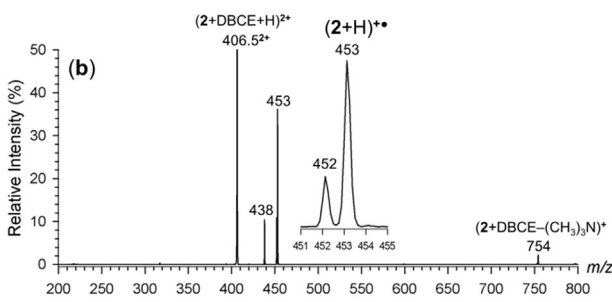


Figure 1. Electron-transfer dissociation mass spectra of a) $(2 + H)^{2+}$ (m/z 226.5), and b) $(2 + H + DBCE)^{2+}$, m/z 406.5.

(m/z 452) and loss of a CH₃ group (m/z 438) and trimethylamine (m/z 394) from the reduced side-chain. To generate a stable cation radical $(2+H)^+$ for action spectroscopy, we resorted to a previously developed technique^[11] that relies on electron-transfer dissociation (ETD)[13] of non-covalent complexes with crown ethers, such as 2,3:11,12-dibenzo-18-crown-6-ether (DBCE). The doubly charged complex, (2+H+DBCE) $^{2+}$, m/z 406.5, was formed readily by electrospray ionization and furnished abundant cation radicals (2+H)+• (m/z 453) by reduction and loss of DBCE upon ETD (Figure 1b). The minor fragment ions by loss of CH₃ from $(2+H)^{+}$ (m/z 438) and loss of $(CH_3)_3N$ from the DBCE complex (m/z 754) were representative of reduction of the fixed charged trimethylammonium group followed by fast dissociation of the hypervalent trimethylammonium radicals.[14] Thus, the surviving $(2+H)^{+}$ cation radical can be unequivocally assigned to an adenine radical in the form of a hydrogen atom adduct. Quite analogous results were obtained for $(1 + H)^{+}$ (m/z 493, Figure S3 a,b), illustrating the similarity of radicals formed by electron transfer to both dications.

The cation-radicals were characterized by CID-MS³ (Figure 2a,b and Figure S4a,b). Upon mild excitation in the ion trap, $(2+H)^{+}$ underwent a loss of an H atom as the sole fragmentation. Upon increasing the excitation amplitude, the (2+H)⁺· ion underwent further dissociation, forming fragment ions that were identical to those in the CID spectrum of 2^+ (Figure 2a, Figure S2b). The dissociations of 2^+ and (2+H)+• were further investigated by deuterium labeling of the six exchangeable protons in $(2-D_5 + D + DBCE)^{2+}$ (m/z 409.5,Figure S5 a). The CID-MS³ spectrum of $(2-D_5+D)^{+1}$ (m/z 459, Figure 2b) revealed > 99% selective loss of D. The absence of loss of a light H atom indicated that the OD, ND_2 , and ND protons in $(2-D_5+D)^{+}$ did not mix with the other adenosine hydrogen atoms, namely, with the ring C-2-H and C-8-H. The results for $(1-D_3+D)^{+\bullet}$ were quite analogous,

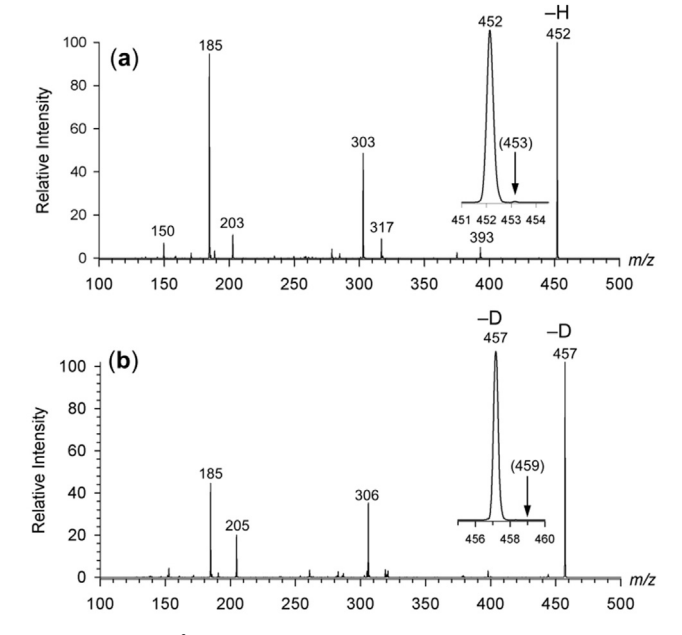


Figure 2. CID-MS³ spectra of a) $(2 + H)^{+}$ (m/z 453), b) $(2-D_5 + D)^{+}$ (m/z 459).

showing an exclusive loss of D from the N-D tagged positions upon CID of the cation radical (Figure S6a,b).

Photodissociation of $(1+H)^{+}$ and $(2+H)^{+}$ across the 210-700 nm wavelength region resulted in the loss of H as a major channel (Figure 3a, Figure S7a,b).

This presented a complication, because loss of H also occurred spontaneously upon storing the cation radicals in the ion trap. Time-dependent measurements, using $(1 + H)^{+}$ and $(2+H)^{+}$ that were thermalized in the ion trap for 150 ms, provided a single-exponential decay curves (Figure S8 a,b), from which we obtained the respective unimolecular rate constants for the spontaneous, thermally driven, loss of H as $k_{\text{H-diss}} = 0.61$ and $0.56 \,\text{s}^{-1}$. Although we did not directly measure the stored ion temperature, previous studies estimated the temperature of trapped ions in the range of 295– 350 K.[15-18] The knowledge of the spontaneous dissociation kinetics allowed us to make background corrections in the UVPD spectra that were obtained on a 100 ms time scale.

The UVPD action spectra of $(1+H)^{+}$ (Figure S7) and $(2 + H)^{+}$ were similar, consisting of four absorption bands. These are illustrated with the spectrum of $(2+H)^{+}$ that displayed maxima at 220, 275, and 325 nm and a broad band stretching from 410 to 600 nm (Figure 3a). Minor channels, chiefly due to secondary dissociations of the m/z 492 primary fragment ion, formed the bands peaking at 260 and 320 nm (Figure 3b). The action spectra of the radicals were quite different from the spectrum of the closed-shell ion 1+ (Figure S9). The action spectrum of $(2 + H)^{+}$ was analogous to the transient absorption spectra of adenine derivatives reported by Candeias and Steenken^[6] that were taken after irradiation in solution. In particular, the absorption spectrum taken 2 µs after irradiation, that was assigned to an Nprotonated adenine radical, showed bands at 315 and 550 nm that were analogous to the 325 and 500 nm bands in the action spectrum. The solution spectrum was found to change with

7773



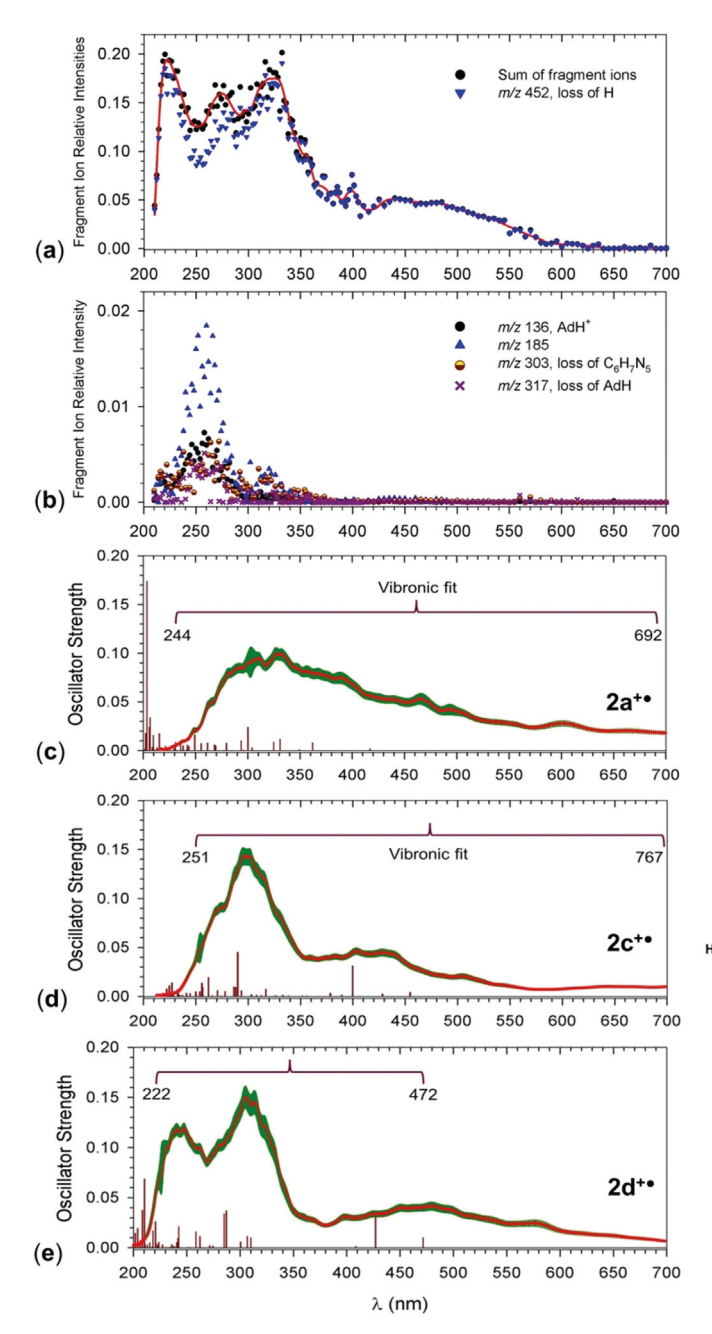


Figure 3. UVPD action spectra of $(2+H)^+$. a) The major photodissociation channel by loss of H at m/z 452. b) Minor photodissociation channels. For fragment ion assignments see Figure 2a and Table S1 (Supporting Information). M06-2X/6-31 + G(d,p) TD-DFT vibronic spectra of c) $2a^+$, d) $2c^+$, and e) $2d^+$ plotted to match the experimental wavelength range. The green bars represent the oscillator strength error in vibronic transitions. The brackets show the wavelength range of TD-DFT excitations (red vertical bars) used for vibronic calculations.

time to develop new bands at 355 and 460 nm that were assigned to a C-8 hydrogen atom adduct.^[6] In contrast, a strong 355-nm band was not observed in the action spectra of gas-phase $(1+H)^{+}$ and $(2+H)^{+}$.

To interpret the UVPD spectra and assign structures, we undertook an extensive computational study of adenosine radicals, cation-radical conjugates and their dication precur-

sors. Theoretical absorption spectra were obtained by time-dependent density functional theory (TD-DFT) M06-2X/6-31 + G(d,p) calculations for the lowest 45 excited states. For 25 excited states, we calculated vibronic transitions from 300 vibrational states populated at 310 K. This covered the wavelength region down to 201-251 nm. Previous benchmark studies established M06-2X/6-31 + G(d,p) TD-DFT calculations as giving an excellent match between the calculated and experimental UV/Vis spectra of nucleobase and nucleoside cation radicals. [19]

Low-energy conformers of protomeric adenosine radical conjugates corresponding to H-atom adducts to N-1 (2a+·), C-2 $(2b^{+})$, N-3 $(2c^{+})$, N-7 $(2d^{+})$ and C-8 $(2e^{+})$ positions in adenine were obtained by a combination of Born-Oppenheimer molecular dynamics for conformational analysis, DFT geometry optimization, and frequency analysis (Figure 4). Computational details are given in the Supporting Information. The relative energies were calculated at several levels of DFT and ab initio theory (Table 1): the M06-2X/6-311++ G(2d,p) energies are discussed in text. The calculations identified the C-8-H adduct 2e+ as the global energy minimum, in agreement with previous calculations of Hatom adducts to adenine. [9,20,21] However, as indicated by the above-described deuterium-labeling experiments, neither $2e^{+\cdot}$ nor the second lowest energy C-2-H adduct $(2b^{+\cdot})$ were formed in the gas phase. Among the N-H adducts, the N-1-H $(2a^{+})$, N-3-H $(2c^{+})$, and N-7-H $(2d^{+})$ isomers showed very

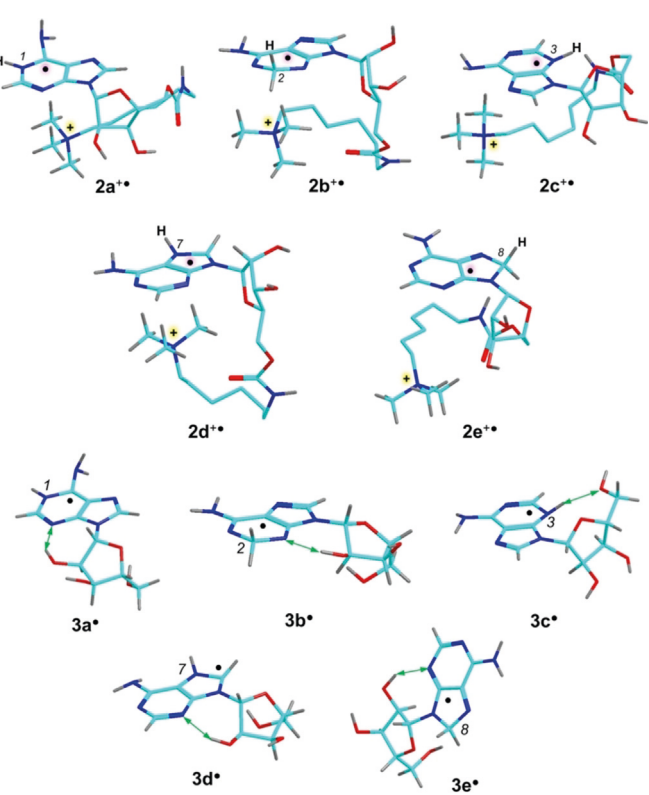


Figure 4. M06-2X/6-31+G(d,p) optimized geometries of cation radical conjugates $2a^+$ - $2e^+$ and adenosine radicals $3a^-3e^-$. Atom color coding is as follows: cyan=C, blue=N, red=O, gray=H. The ribose and side-chain C-H hydrogens are not shown for $2a^+$ - $2e^+$. Green arrows indicate hydrogen bonds.

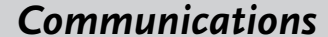






Table 1: Relative energies of adenosine cation-radical conjugates.

Species/reac- tion	Relative energy ^(a,b)				
	M06-2X ^[c]	ωB97X-D	$PMP2^{[d]}$		
	6-311 ++ G(2d,p)	6-31 + G- (d,p)	6-311 ++ G (2d,p)		
2 a+•	11 (5.5)	12	-0.3		
2 b+•	-21 (-20)	-24	-22		
2 c+•	-7.7 (-3.7)	-9.6	-11		
2 d ⁺ •	0 (0)	0	0		
2 e ⁺ •	-47 (-48)	-52	-47		
$2d^+ \rightarrow 2^+ + H^-$	67 (42)	81	27		
2 a ⁺ •→syn-TS2a	81	100	82		
2 a ⁺ • → anti-TS2a	98	109	85		
2b +•→syn-TS2b	120	138	101		
$\mathbf{2b}^{+\bullet}$ \rightarrow anti-TS2b	120	137	95		
$2c^{+}$ \rightarrow syn-TS2c	120	138	125		
$2c^{+}$ \rightarrow anti-TS2c	121	142	107		
2 d ⁺ •→syn-TS2d	95	109	88		
$2d^{+\bullet}$ \rightarrow anti-TS2d	106	117	90		
$2e^{+}$ \rightarrow syn-TS2e	141	161	125		
$2e^{+\bullet}$ \rightarrow anti-TS2e	142	61	120		

[a] In kJ mol $^{-1}$. [b] Including B3LYP/6-31 + G(d,p) zero-point energies scaled by 0.975 and referring to 0 K unless stated otherwise. [c] Relative free energies at 310 K in parentheses. [d] From spin-projected MP2/6-311 + + G(2d,p) calculations.

similar relative free energies (Table 1), indicating no particular thermodynamic preference for either form. We note that the use of M06-2X relative energies was corroborated by a parallel study of H-atom adducts to adenosine for which we obtained benchmark CCSD(T) energies extrapolated to the complete basis set (Table 2). The adenosine radical data pointed to an excellent match between the M06-2X/6-311++ G(2d,p) and CCSD(T)/CBS relative energies with the rootmean-square and maximum deviations of 3.3 and 6.0 kJ mol $^{-1}$, respectively.

Table 2: Relative energies of adenosine radicals.

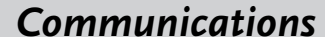
Radical/reac- tion	Relative energy ^[a,b]				
	M06-2X ^[c] 6-311 ++ G- (2d,p)	PMP2 ^[c,d]	CCSD(T) ^[c,e] aug-cc- pVTZ	CCSD(T) ^[c,f,g] CBS	
3 a [.]	7.2	-1	5.5	5.2 (0.1)	
3 p.	-18	-21	-23	-20 (-23)	
3 c [.]	20	17	21	22 (18)	
3 d [.]	0	0	0	0(0) ^[f]	
3 e'	-53	-51	-54	-52 (-55)	
$3 d \cdot \rightarrow 5 + H \cdot$	66	28	64	64 (36)	
3 a⁺ →TS3a	92	81	92	95	
3 c ⁺→TS3c	95	86	97	97	
3 d •→TS3d	101	85	99	100	

[a] In kJ mol $^{-1}$. [b] Including zero-point energies and referring to 0 K unless stated otherwise. [c] Single-point energy calculations on M06-2X/6-31+G(d,p) optimized geometries. [d] From spin-projected MP2/6-311++G(2d,p) calculations. [e] From basis set expansion: E[CCSD(T)/aug-cc-pVTZ] \approx E[CCSD(T)/aug-cc-pVDZ]+E[PMP2/aug-cc-pVTZ]-E[PMP2/aug-cc-pVDZ]. [f] Extrapolated to the complete basis set. [g] Relative free energies at 310 K in parentheses.

The calculated vibronic spectra of $2a^+$, $2c^+$, and $2d^+$ are shown in Figure 3c-e. The spectra of 2b+ and 2e+ are displayed in Figure S10a,b for comparison. The N-1-H adduct 2a⁺ showed a broad featureless band resulting from multiple excitations in the 244–692 nm range (Figure 3c). In addition, the spectrum showed a strong transition at 204 nm that was outside the range for vibronic analysis but was expected to give rise to a strong narrow band at ca. 210 nm. The N-3-H adduct 2c⁺ showed two major bands with maxima at 300 and 400 nm along with broad bands at 440 and 500 nm (Figure 3 d). The N-7-H adduct 2d+ showed two major bands with maxima at 240 and 310 nm along with a broad band peaking at 480 nm and extending to above 600 nm (Figure 3e). The C-2-H adduct 2b⁺ displayed a spectrum consisting of a band composed of vibronically broadened transitions in the 201-567 nm range that was substantially different from the spectrum of the C-8-H adduct 2e⁺, which showed prominent bands with maxima at 240, 320, and 340 nm (Figure S10 a,b). The calculated spectra of $2b^{+}$, $2d^{+}$, and $2e^{+}$ displayed bands that were apparent in the action spectrum of $(2+H)^{+}$ (Figure 3a), with the closest match for 2d⁺. In addition, the sharp band at 220 nm in the action spectrum (Figure 3a) was represented by the intense transitions at 208 and 210 nm in the TD-DFT spectrum of 2d⁺ (Figure 3e). Considering that 2b⁺ and 2e⁺ were excluded on the basis of deuterium labeling, the action spectrum can be unambiguously assigned to the N-7-H adduct 2d⁺ as the dominant component. Because the absorption bands of thermal ions are broad, we cannot exclude the presence of very minor amounts of the $2a^{+}$ and $2c^{+}$ whose bands, if present, would be obscured by those from the dominant isomer $2d^+$.

The adenosine cation-radical conjugates under study had a fixed-charge group that is absent in natural adenosine radicals, and so we investigated the effect of the fixed charge on the radical equilibrium geometries, electronic structure, and excited states. Cation radicals 2a+, 2b+, 2c+, and 2d+ favored conformations in which the charged trimethylammonium group was stacked underneath the purine ring (Figure 4). The proximate methyl and methylene hydrogen atoms were within their combined van der Waals radii distance from the adenine ring C and N atoms, e.g., N-3 and C-6 in $2a^{+}$, N-1 and C-2 in $2b^{+}$, NH₂ in $2c^{+}$, and C-2 and N-7 in 2d⁺ (Figure 4). This attractive intramolecular interaction replaced hydrogen bonding of the 2' and 5'-hydroxyls to the purine nitrogen atoms that was prominent in low-energy conformers of adenosine radicals 3a-3e (Figure 4). However, the different conformations of $2a^+-2e^+$ and $3a^--3e^+$ had only a minor effect on the electronic structure and excited states. The ground electronic states in all these radicals and cation radicals had the unpaired electron in the singlyoccupied molecular orbitals (SOMO) of the π_z type that were delocalized over the purine ring, as illustrated with 2d+ and **3d'** (Figure 5) in which the SOMO π_z orbitals showed the same nodality. The first excited states (A) in both $2d^{+}$ $(\Delta E_{\rm exc} = 2.63 \text{ eV})$ and $3 \text{ d} \cdot (\Delta E_{\rm exc} = 2.74 \text{ eV})$ involved electron promotion to a combination of virtual π_z^* orbitals of very similar nodality. A minor difference in the ordering of excited states concerned the weak transition to the C state in $2d^+$. $(\Delta E_{\rm exc} = 3.03 \text{ eV})$ that appeared as the **B** state in **3d** $(\Delta E_{\rm exc} =$

7775







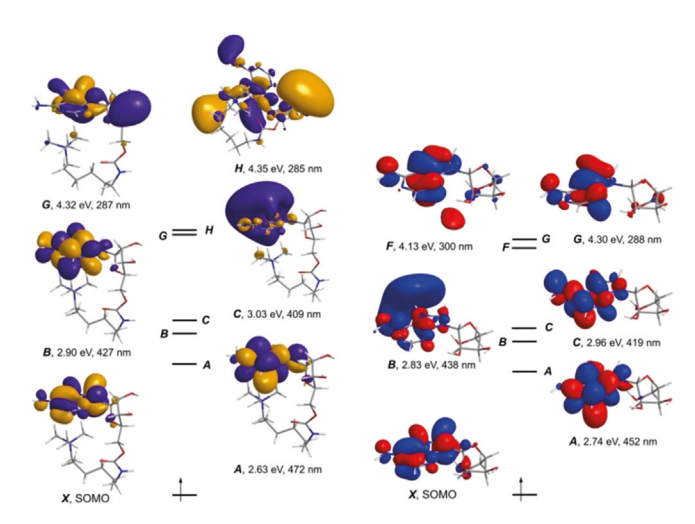


Figure 5. Molecular orbital representation of low excited electronic states in adenosine conjugate $2d^{+}$ (left panel) and adenosine radical $3d^{\cdot}$ (right panel).

2.83 eV. In each case, these states contained substantial components of Rydberg orbitals (Figure 5). The intense transitions at $\Delta E_{\rm exc} = 2.90$ eV (\boldsymbol{B} state in $2\mathbf{d}^{+*}$) and $\Delta E_{\rm exc} = 2.96$ eV (\boldsymbol{C} state in $3\mathbf{d}^{*}$) (Figure S11) as well as the \boldsymbol{G} ($2\mathbf{d}^{+*}$) and \boldsymbol{F} ($3\mathbf{d}^{*}$) states involved virtual π_z^* orbitals of very similar nodality for the cation radical and adenosine radical. Very similar assignment of excited states was made for $2\mathbf{a}^{+*}$ and $3\mathbf{a}^{*}$ (Figure S12), $2\mathbf{b}^{+*}$ and $3\mathbf{b}^{*}$ (Figure S13), and $2\mathbf{e}^{+*}$ and $3\mathbf{e}^{*}$ (Figure S14). The N-3-H adducts $2\mathbf{c}^{+*}$ and $3\mathbf{c}^{*}$ were exceptional in that the spectrum of the latter showed transitions to Rydberg states at 2.19, 2.44, and 2.61 eV that had no equivalents in the spectrum of $2\mathbf{c}^{+*}$ (Figure S15).

The facile loss of H from $(1+H)^{+\cdot}$ and $(2+H)^{+\cdot}$ was further investigated by obtaining transition state (TS) geometries and energies for adenine C–H and N–H bond dissociations in $2a^{+\cdot}$, $2b^{+\cdot}$, $2c^{+\cdot}$, $2d^{+\cdot}$, and $2e^{+\cdot}$ (Figures S16 and S17) and for analogous dissociations in adenosine radicals $3a^{\cdot}$ 3c, and 3d (Figure S18, Tables 1 and 2). The benchmark TS energies for the cleavage of the N-1-H, N-3-H, and N-7–H bonds in $3a^{\cdot}$, $3c^{\cdot}$, and $3d^{\cdot}$ were low, ranging between 95–100 kJ mol⁻¹, and showing the weak trend E[TS(N-1-H)] \leq E[TS(N-3-H)] \leq E[TS(N-7-H)]. Again, the M06-2X-calculated TS energies closely followed the CCSD(T)/CBS benchmarks (Table 2).

The stacked side chains in the cation radicals made the X–H bond dissociations in $2\mathbf{a}^{+}$ - $2\mathbf{e}^{+}$ diastereotopic, leading to syn and anti-facial transition states of distinct geometries and energies. This effect was most pronounced for the syn and anti-facial N–H bond dissociations in $2\mathbf{a}^{+}$, $2\mathbf{c}^{+}$, and $2\mathbf{d}^{+}$ (Figure S16). In contrast, the calculated TS energies for the syn and anti-facial C–H bond dissociations in $2\mathbf{b}^{+}$ and $2\mathbf{e}^{+}$ were nearly identical (Table 1). Regarding the N-7–H bond dissociations in the experimentally observed isomer $2\mathbf{d}^{+}$, the syn-facial TS (syn-TS2d) was found at a shorter N-7-H distance (1.485 Å) and lower energy than the anti-facial TS (anti-TS2d, Figure S16), which was at $d(N-7\cdots H) = 1.525$ Å. This effect could not be attributed to different electron distributions in the TS, which were nearly identical for the syn

and *anti*-facial TS. However, *syn*-TS2d showed a larger displacement of the departing H atom from the ring plane than did *anti*-TS2d, allowing a more efficient atomic orbital overlap in the adenine ring HOMO as it was developing in the course of dissociation.

The calculated TS energies were used for transition-state theory (TST) calculations of unimolecular rate constants for the H-atom loss to be compared with the experimental value of $k = 0.56 \,\mathrm{s}^{-1}$. The TST rate constants calculated for the syn and anti N-3-H dissociations were too low ($< 10^{-4} \, \text{s}^{-1}$ at 360 K) to be compatible with the experimental value. The rate constants for the syn- and anti-N-1-H dissociations, which had low calculated TS energies (Table 1), were affected by negative activation entropies, $\Delta S^{\dagger} = -16.4$ and −29.7 J mol⁻¹ K⁻¹, respectively, at 360 K. These rate constants are shown in Figure S19 a. The rate constant calculated for the syn-TS2d energy (95 kJ mol⁻¹, Table 1) matched the experimental value for an effective ion temperature of 351 K (Figure S19b). Considering the estimated $\pm 3 \text{ kJ mol}^{-1}$ accuracy of the calculated TS energy, the range of ion effective temperatures giving matching TST rate constants can be expanded to 340-362 K. This fits within or is close to previous estimates of the effective temperature of ions stored in radiofrequency ion traps.^[15-18] Thus, the calculated dissociation kinetics of the N-7-H adduct 2d+ was compatible with the experimental result.

In summary, a new method for the generation of charge-tagged nucleoside radicals has been developed that was combined with photodissociation action spectroscopy of well-defined transient molecular species in the gas phase. As illustrated with adenine riboside, the charge-tagged radicals are electronically equivalent to natural nucleoside radicals, and derivatization of the 2' and 3'-OH groups in $(1+H)^{+}$ by a non-polar group has a negligible effect on the electronic properties of the radicals. Thus, the method has the potential of being applied to the other nucleosides relevant to electron transfer in DNA and RNA to provide electronic structure of reactive intermediates pertinent to the early stages of ionization damage.

Acknowledgements

This research was supported by the NSF Grant CHE-1661815.

Conflict of interest

The authors declare no conflict of interest.

Keywords: charge-tagged adenosine radicals \cdot H-loss kinetics \cdot transition states \cdot UV/Vis action spectroscopy \cdot vibronic spectra

How to cite: Angew. Chem. Int. Ed. 2020, 59, 7772–7777 Angew. Chem. 2020, 132, 7846–7851

^[1] D. E. Holmes, R. B. Ingalls, L. S. Myers, Jr., *Int. J. Radiat. Biol.* **1967**, *13*, 225–234.

GDCh

Communications



- [2] P. N. Moorthy, E. Hayon, J. Am. Chem. Soc. 1975, 97, 3345– 3350.
- [3] A. Hissung, C. von Sonntag, D. Veltwisch, K.-D. Asmus, *Int. J. Radiat. Biol.* 1981, 39, 63-71.
- [4] K. J. Visscher, M. P. De Haas, H. Loman, B. Vojnovic, J. M. Warman, Int. J. Radiat. Biol. 1987, 52, 745-753.
- [5] M. D. Sevilla, R. Failor, C. Clark, R. A. Holroud, M. Pettei, J. Phys. Chem. 1976, 80, 353–358.
- [6] L. P. Candeias, S. Steenken, J. Phys. Chem. 1992, 96, 937-944.
- [7] J. Barnes, W. A. Bernhard, J. Phys. Chem. 1993, 97, 3401 3408.
- [8] J. Barnes, W. A. Bernhard, J. Phys. Chem. 1994, 98, 10969– 10977.
- [9] X. Chen, E. A. Syrstad, M. T. Nguyen, P. Gerbaux, F. Tureček, J. Phys. Chem. A 2005, 109, 8121 – 8132.
- [10] C. Yao, M. Cuadrado-Peinado, M. Polášek, F. Tureček, Angew. Chem. Int. Ed. 2005, 44, 6708-6711; Angew. Chem. 2005, 117, 6866-6869.
- [11] J. A. Korn, J. Urban, A. Dang, H. T. H. Nguyen, F. Turecek, J. Phys. Chem. Lett. 2017, 8, 4100 – 4107.
- [12] "Laser Photodissociation and Spectroscopy of Mass-Separated Biomolecular Ions": R. Antoine, P. Dugourd, in *Lecture Notes in Chemistry, Vol. 83* (Eds.: N. C. Polfer, P. Dugourd), Springer, Heidelberg, **2013**, pp. 93–116.

- [13] J. E. P. Syka, J. J. Coon, M. J. Schroeder, J. Shabanowitz, D. F. Hunt, Proc. Natl. Acad. Sci. USA 2004, 101, 9528-9533.
- [14] S. A. Shaffer, F. Tureček, J. Am. Chem. Soc. 1994, 116, 8647– 8653
- [15] D. E. Goeringer, S. A. McLuckey, J. Chem. Phys. 1996, 104, 2214–2221.
- [16] S. Gronert, J. Am. Soc. Mass Spectrom. 1998, 9, 845 848.
- [17] E. R. Lovejoy, R. R. Wilson, J. Phys. Chem. A 1998, 102, 2309 2315.
- [18] W. A. Donald, G. N. Khairallah, R. A. J. O'Hair, J. Am. Soc. Mass Spectrom. 2013, 24, 811–815.
- [19] A. Dang, Y. Liu, F. Tureček, J. Phys. Chem. A 2019, 123, 3272– 3284
- [20] J. Reynisson, S. Steenken, Phys. Chem. Chem. Phys. 2005, 7, 659-665.
- [21] S. D. Wetmore, R. J. Boyd, L. A. Eriksson, J. Phys. Chem. B 1998, 102, 10602-10614.

Manuscript received: December 23, 2019 Revised manuscript received: January 22, 2020 Accepted manuscript online: February 11, 2020 Version of record online: March 16, 2020